Shap. Mem. Superelasticity (2017) 3:218–229
DOI 10.1007/s40830-017-0116-1

SPECIAL ISSUE: ICFSMA 2016, INVITED PAPER

Optimizing Magnetocaloric Properties of Heusler-Type Magnetic Shape Memory Alloys by Tuning Magnetostructural Transformation Parameters

Lian Huang[1,2] · Yuhai Qu[1] · Daoyong Cong[1] · Xiaoming Sun[1] · Yandong Wang[1]

Published online: 7 August 2017

Abstract Heusler-type magnetic shape memory alloys show a magnetostructural transformation from the low-magnetization phase to the high-magnetization phase upon the application of external magnetic fields. As a result, these alloys exhibit fascinating multifunctional properties, such as magnetic shape memory effect, magnetocaloric effect, magnetoresistance, and magnetic superelasticity. All these functional properties are intimately related to the coupling of the structural and magnetic transitions. Therefore, deliberate tuning of the magnetostructural transformation parameters is essential for obtaining optimal multifunctional properties. Here, we show that by tuning the magnetostructural transformation parameters, we are able to achieve a variety of novel magnetocaloric properties with different application potentials: (1) large magnetic entropy change of 31.9 J kg^{-1} K^{-1} under a magnetic field of 5 T; (2) giant effective magnetic refrigeration capacity (251 J kg^{-1}) with a broad operating temperature window (33 K) under a magnetic field of 5 T; (3) large reversible field-induced entropy change (about 15 J kg^{-1} K^{-1}) and large reversible effective magnetic refrigeration capacity (77 J kg^{-1}) under a magnetic field of 5 T. The balanced tuning of magnetostructural transformation parameters of magnetic shape memory alloys may provide an instructive reference to the shape memory and magnetic refrigeration communities.

✉ Daoyong Cong
dycong@ustb.edu.cn

[1] State Key Laboratory for Advanced Metals and Materials, University of Science and Technology Beijing, No. 30 Xueyuan Road, Haidian District, Beijing 100083, People's Republic of China

[2] Hunan Institute of Engineering, Xiangtan 411104, People's Republic of China

Keywords Magnetic shape memory alloys · Magnetostructural transformation · Magnetocaloric effect · Martensitic transformation

Introduction

On account of environmental concerns and the limited thermodynamic efficiency of the traditional refrigeration technology based on vapor compression, magnetic refrigeration technology based upon the magnetocaloric effect (MCE) has generated a worldwide interest during the past decades [1, 2]. Magnetic refrigeration technology would thoroughly avoid the utilization of ozone-depleting volatile refrigerants usually used in the traditional refrigerators [3]. Furthermore, the efficiency of magnetic refrigeration technology is expected to exceed the efficiency of vapor compression technology, resulting in much reduction in energy consumption compared with traditional technologies [4]. The search for optimal magnetocaloric materials is a crucial parameter in the development of magnetic refrigeration technology. Up to now, several alloy systems showing magnetostructural transformation and giant MCE have been discovered, like Gd–Si–Ge [5], La–Fe–Si [6], Fe–Rh [7], Mn–Fe–P–As [8], Mn–Co–Ge [9], and Ni–Mn–*X*-based (X = Sn, In, Sb, Ga) magnetic shape memory alloys [10–13]. Among them, Ni–Mn–*X*-based (X = Sn, In, Sb, Ga) magnetic shape memory alloys are considered to be promising candidates for magnetic refrigeration applications thanks to their fascinating MCE, relatively low cost of raw elements, and non-toxicity. In addition to fascinating MCE, these Heusler alloys also show other interesting multifunctional properties, like magnetic shape memory effect [14], magnetoresistance [15], and elastocaloric effect [16]. The multifunctional properties make

these magnetic shape memory alloys have the great potential to be used in a wide range of applications from actuators and sensors to solid-state refrigeration. Recently, many efforts have been spent on developing high-performance magnetocaloric materials in Ni–Mn–*X*-based (X = In, Sn, Sb, Ga) magnetic shape memory alloys [17–20]. However, there are still several standing problems that need to be resolved urgently. For these alloys, the large ΔS is usually obtained in a limited operating temperature window. Moreover, reproducible MCE cannot be achieved during the magnetic field cycling.

For a given material, the magnitude of MCE is directly linked to the fraction of material which undergoes the martensitic transformation or reverse transformation when the applied magnetic field is applied or removed [21]. The minimum applied field $\Delta(\mu_0 H)_{\text{com}}$ required to induce the complete (denoted as "com") magnetostructural transformation can be expressed as $\Delta(\mu_0 H)_{\text{com}} = \Delta T_{\text{int}}/(\Delta T/\mu_0 \Delta H)$, where ΔT_{int} is the phase transformation interval and $\Delta T/\mu_0 \Delta H$ is the sensitivity of phase transformation temperatures to applied magnetic field [19]. However, irreversibility of the magnetostructural transformation is commonly encountered due to the thermal and magnetic hysteresis, which will reduce the effective value of MCE during the second and subsequent field cycles [11]. The irreversibility of MCE in these alloys strictly limits their utilization in magnetic refrigeration applications. Actually, the minimum applied field $\Delta(\mu_0 H)_{\text{com-rev}}$ needed to induce the complete and reversible (denoted as "com-rev") magnetostructural transformation can be expressed as $\Delta(\mu_0 H)_{\text{com-rev}} = (\Delta T_{\text{hys}} + \Delta T_{\text{int}})/(\Delta T/\mu_0 \Delta H)$, where ΔT_{hys} is the thermal hysteresis [19]. Additionally, it was well demonstrated in literature that the ΔT_{int}, ΔT_{hys}, and $\Delta T/\mu_0 \Delta H$ increase simultaneously with the decrease of phase transformation temperature caused either by magnetic field or by composition variation [22]. On the other hand, $\Delta T/\mu_0 \Delta H$ equals to $\Delta M/\Delta S_{\text{tr}}$ according to the Clausius–Clapeyron relation, where ΔM is the magnetization difference between austenite and martensite across transformation and ΔS_{tr} is the transformation entropy change, and ΔS_{tr} corresponds to the maximum obtainable magnetic entropy change, an important parameter characterizing the MCE. If ΔS_{tr} is large, the $\Delta T/\mu_0 \Delta H$ is reduced and a high magnetic field is required to obtain a reasonably large MCE. If ΔS_{tr} is small, the $\Delta T/\mu_0 \Delta H$ is enhanced and the required field is lowered, but the attainable MCE is reduced. Thus, it is an arduous task to optimize magnetocaloric properties of a given material. The challenge for optimizing the magnetocaloric properties of Ni–Mn-based magnetic shape memory alloys is the best balanced tuning of ΔT_{hys}, ΔT_{int}, and $\Delta T/\mu_0 \Delta H$.

In this paper, we present a brief review of our recent progress in exploring Ni–Mn-based magnetic shape memory alloys with a variety of novel magnetocaloric properties for different application potentials by the balanced tuning of all the magnetostructural transformation parameters (phase transformation temperature, ΔT_{hys}, ΔT_{int}, ΔM, ΔS_{tr}, etc.). This paper is organized as follows: In Sect. 2, we briefly introduce the methods for estimation of magnetic entropy change ΔS_{m}, refrigeration capacity RC, and the effective refrigeration capacity RC_{eff}. In Sect. 3, we review a variety of Ni–Mn-based magnetic shape memory alloys with different features for different application potentials: (1) large magnetic entropy change of 31.9 J kg^{-1} K^{-1} under a magnetic field of 5 T [23]; (2) giant effective magnetic refrigeration capacity (251 J kg^{-1}) with a broad operating temperature window (33 K) under a magnetic field of 5 T [24]; (3) large reversible magnetic entropy change (ΔS_{m}) of 14.6 J kg^{-1} K^{-1} and large reversible effective refrigeration capacity (76.6 J kg^{-1}) under 5 T [25]. In Sect. 4, we give some conclusions and extension remarks.

Methods for Estimation of ΔS_{m}, RC, and RC_{eff}

The MCE is mainly characterized by the adiabatic temperature change ΔT_{ad} and isothermal entropy change ΔS_{m}. ΔT_{ad} can be determined by calorimetric measurements under magnetic fields [7] or direct adiabatic temperature measurement. However, these measurements are very complex, so the MCE is usually reported in terms of ΔS_{m} that can be calculated based on isothermal magnetization measurements with the aid of the Maxwell relation [8, 17]. In order to estimate the ΔS_{m}, the $M(H)$ curves at different temperatures approaching the austenitic transformation temperature should be measured. Before each $M(H)$ measurement, the sample must be first cooled to a certain temperature ($<M_{\text{f}}$) to ensure the same initial state of a fully transformed martensite and then heated to the target temperature. Based on the $M(H)$ data, ΔS_{m} can be estimated using the Maxwell relation [8, 17]:

$$\Delta S_m = S_m(T,H) - S_m(T,0) = \int_0^{\mu_0 H} \frac{\partial M}{\partial T} d(\mu_0 H). \quad (1)$$

It should be noted that currently it is questionable whether the calculation using the Maxwell relation could yield reliable ΔS_{m} values for first-order magnetostructural transformation due to the coexistence of martensite and austenite [26]. In order to check the validity of the calculated results, the ΔS_{m} values should also be estimated with the Clausius–Clapeyron relation which can be used to correctly determine the magnetic field-induced entropy change associated with the metamagnetic transition [27]:

$$\Delta S_{\mathrm{m}} = -\Delta M' \cdot \frac{\mathrm{d}H_{\mathrm{cr}}}{\mathrm{d}T}, \quad (2)$$

where H_{cr} is the critical field value of the inflection point within the metamagnetic transition region and $\Delta M'$ corresponds to the magnetization difference between the high and low field phases, which can be evaluated from the isothermal $M(H)$ curves. If the results obtained from the Clausius–Clapeyron relation and the Maxwell relation are consistent, it can be confirmed that the ΔS_{m} values are reliable.

For practical applications, the magnetic cooling efficiency considering not only the magnitude of the MCE but also the operating temperature range is another figure of merit for judging the potential of the magnetic refrigerants [28]. The refrigeration capacity (RC) which stands for the amount of thermal energy that can be transferred between the cold and hot sinks in one thermodynamic cycle, is defined as

$$RC = \int_{T_{cold}}^{T_{hot}} \Delta S_m dT, \quad (3)$$

where T_{cold} and T_{hot} are the corresponding temperatures at half maximum of the ΔS_{m} versus temperature (T) curve. It can be estimated by numerically integrating the area under the $\Delta S_{\mathrm{m}} \sim T$ curve between T_{cold} and T_{hot}.

For justifying the usefulness of a magnetic refrigerant during a thermodynamic cycle, the magnetic hysteresis loss (estimated from the area between the $M(H)$ curves measured during increasing and decreasing fields) must be taken into account. Accordingly, a more reasonable criterion for assessing the cooling efficiency is the effective refrigeration capacity $\mathrm{RC_{eff}}$ which can be obtained by subtracting the average hysteresis loss ($\overline{HL}$) from the RC value [28]

$$RC_{eff} = RC - \overline{HL}. \quad (4)$$

Optimization of Magnetocaloric Performance

Large Magnetic Entropy Change in a $Ni_{41}Co_9Mn_{40}Sn_{10}$ Magnetic Shape Memory Alloy

For practical applications, magnetocaloric materials should have large ΔS_{m}. Although large ΔS_{m} has been reported in many Ni–Mn-based alloys [29–33], the values of ΔS_{m} were just computed from the Maxwell relation and they were not compared with the results estimated from DSC measurements or from the Clausius–Clapeyron relation or from the temperature dependence of specific heat capacity at different magnetic fields. Those results might be unreliable. Thus, it is necessary to discover Ni–Mn–X-based (X = In, Sn, Sb, Ga) magnetocaloric materials with a large and reliable ΔS_{m}. It is known that, for magnetocaloric materials with a first-order phase transformation, the maximum ΔS_{m} that can be obtained is almost equivalent to the transformation entropy change ΔS_{tr} and the structural contribution to ΔS_{tr} is proportional to the unit cell volume change $\Delta V/V$ (ΔV is the volume difference between high-temperature and low-temperature phases, V is the unit cell volume of the high-temperature phase) across the phase transformation. Therefore, in order to obtain large ΔS_{m}, it is important develop new Ni–Mn–X-based (X = In, Sn, Sb, Ga) magnetocaloric materials with large $\Delta V/V$ and optimize the existing Ni–Mn–X-based (X = In, Sn, Sb, Ga) magnetocaloric materials with large $\Delta V/V$.

The $Ni_{45}Co_5Mn_{40}Sn_{10}$ alloy was reported to exhibit large ΔM and large ΔS_{tr} [34]. However, this alloy has a major drawback for MCE applications; that is, the $\Delta(\mu_0 H)_{\mathrm{com}}$ is relatively large (larger than 7 T) due to the small $\Delta T/\mu_0 \Delta H$. In Ni–Mn-based alloys, the Co substitution for Ni was proved to be an effective way to enhance $\Delta T/\mu_0 \Delta H$ [35]. In order to enhance the $\Delta T/\mu_0 \Delta H$ of this particular alloy, we continue to increase the Co content in the $Ni_{45}Co_5Mn_{40}Sn_{10}$ alloy. The DSC curves of the $Ni_{50-x}Co_xMn_{40}Sn_{10}$ (x = 6, 7, 8, and 9) alloys are shown in Fig. 1. We found that when the Co content reaches 9 at.% the martensitic transformation temperature is lower than the Curie temperature of austenite (about 433 K, determined from the DSC curve in Fig. 1) and the difference between them is moderate, indicating $\Delta T/\mu_0 \Delta H$ is significantly enhanced [35], but its ΔS_{tr} is still large ($\approx$32.1 J kg^{-1} K^{-1}).

In order to determine $\Delta T/\mu_0 \Delta H$ and $\Delta(\mu_0 H)_{\mathrm{com}}$ in the $Ni_{41}Co_9Mn_{40}Sn_{10}$ alloy, we carried out isofield

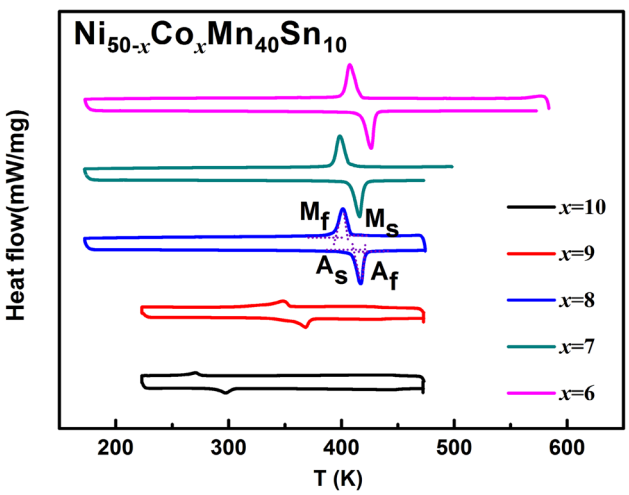

Fig. 1 DSC curves of the $Ni_{50-x}Co_xMn_{40}Sn_{10}$ (x = 6, 7, 8, and 9) alloys

magnetization measurements. Figure 2 shows the temperature dependence of magnetization [*M(T)* curve] measured under 0.01 T and 4 T, respectively. According to the *M(T)* curve under 0.01 T, M_s, M_f, A_s, and A_f, are 351, 339, 357, and 368 K, respectively. Compared with A_s under 0.01 T, the A_s is decreased by 11 K under 4 T, with a rate of $\Delta A_s/\mu_0\Delta H = 2.75$ K/T. As can be seen from Fig. 2, the high-temperature austenite shows ferromagnetic feature while the low-temperature martensite exhibits weak magnetic state. A large magnetization difference ($\Delta M \approx 90$ emu/g as determined from the *M(T)* curve under 4 T) between the two phases across magnetostructural transformation can be observed. The $\Delta(\mu_0 H)_{com}$ is determined to be about 4 T according to $\Delta(\mu_0 H)_{com} = (A_f - A_s)/(\Delta T/\mu_0\Delta H)$. Based on the Clausius–Clapeyron relation $\Delta T/\mu_0\Delta H = \Delta M/\Delta S_{tr}$ [14], ΔS_{tr} under 4 T can be determined to be 32.7 J kg^{-1} K^{-1}, which agrees well with the result determined from DSC measurements ($\approx$ 32.1 J kg^{-1} K^{-1}).

In order to determine the ΔS_m, we measured the *M(H)* curves at different temperatures close to the austenitic transformation temperature, as shown in Fig. 3. As can be seen from this figure, the slope of *M(H)* curves changes abruptly at a critical magnetic field in the temperature range from 344 K to 364 K, indicating the occurrence of magnetic field-induced transformation from martensite to austenite. We estimated the ΔS_m using the Maxwell relation [Eq. (1)] from the *M(H)* curves. The temperature dependence of the estimated ΔS_m at different magnetic fields is illustrated in Fig. 4. It can be found that the maximum value of ΔS_m under 5 T is about 31.9 J kg^{-1} K^{-1} at 358 K. As indicated from Fig. 3, the magnetic field-induced transformation is complete around 358 K; so in this case, the ΔS_m should be comparable to the ΔS_{tr} determined from DSC. As a matter of fact, the ΔS_m (31.9 J kg^{-1} K^{-1}) is indeed close to ΔS_{tr}

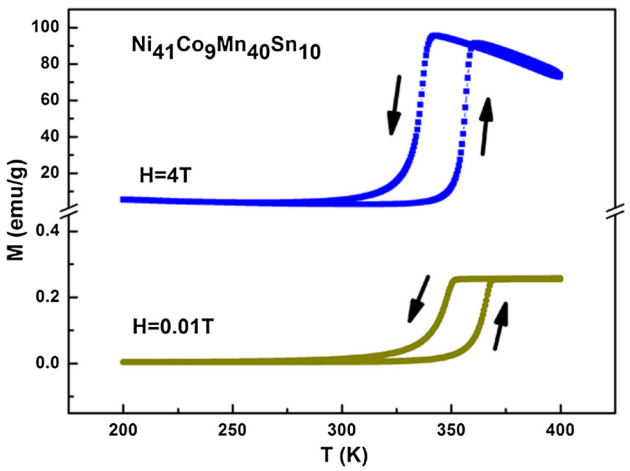

Fig. 2 *M(T)* curves measured under magnetic fields of 0.01 and 4 T, respectively, for the $Ni_{41}Co_9Mn_{40}Sn_{10}$ alloy. Adapted from [23]

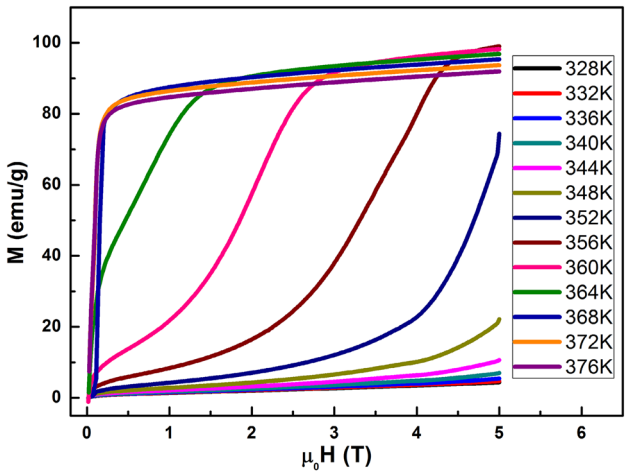

Fig. 3 *M(H)* curves measured at different temperatures close to the austenitic transformation temperature, for the $Ni_{41}Co_9Mn_{40}Sn_{10}$ alloy. Adapted from [23]

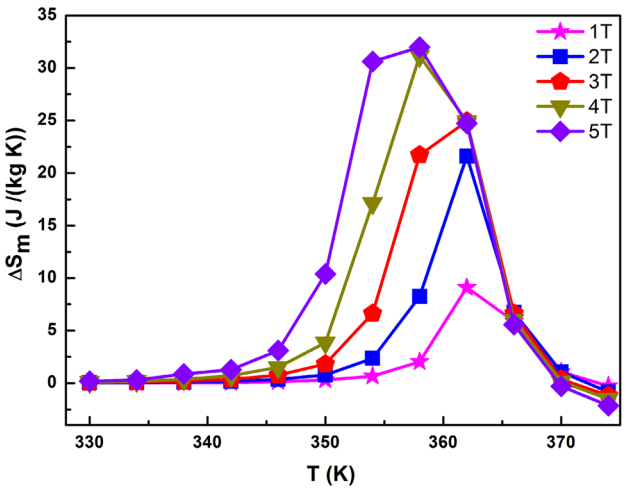

Fig. 4 The magnetic entropy change (ΔS_m) as a function of temperature at different magnetic fields, for the $Ni_{41}Co_9Mn_{40}Sn_{10}$ alloy. Adapted from [23]

($\approx$ 32.1 J kg^{-1} K^{-1}), confirming that the maximum ΔS_m we achieved is reliable. This ΔS_m (31.9 J kg^{-1} K^{-1} under 5 T) is among the highest values reported so far in Ni–Mn–Sn-based alloys [23].

To shed light on the origin of the large ΔS_m (which is related to the large ΔS_{tr}) obtained in our $Ni_{41}Co_9Mn_{40}Sn_{10}$ alloy, we performed in situ synchrotron high-energy X-ray diffraction (HEXRD) experiments. The HEXRD results are shown in Fig. 5. All the diffraction peaks of the austenite can be well indexed according to the $L2_1$-type cubic Heusler structure (Fig. 5a); the diffraction pattern of martensite can be well indexed according to the six-layered modulated (6 M) monoclinic structure [36] (Fig. 5b). Based on the lattice parameter changes determined from

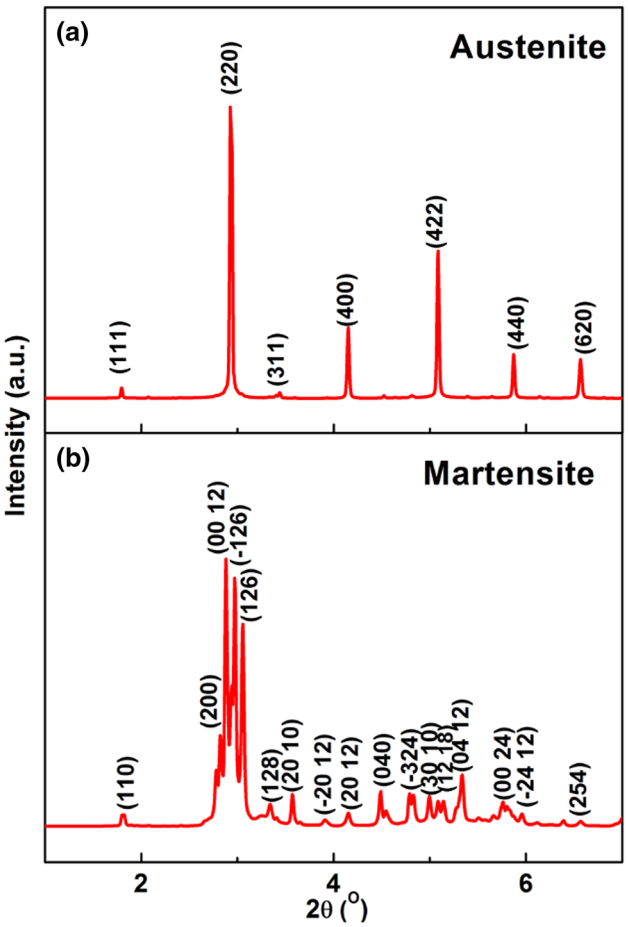

Fig. 5 **a**, **b** High-energy X-ray diffraction patterns experimentally collected at 400 K (**a**) and 100 K (**b**) corresponding to austenite and martensite phases, respectively, for the $Ni_{41}Co_9Mn_{40}Sn_{10}$ alloy. Adapted from [23]

the HEXRD results during the heating process, a significant unit cell volume contraction of 1.31% was found.

As mentioned above, for first-order magnetostructural transformation, the structural part of the transformation entropy change is proportional to the unit cell volume change across phase transformation. Therefore, the significant unit cell volume change ($\approx$1.31%) lies at the origin of the large structural entropy change and, consequently, large magnetic entropy change was observed in the presently studied alloy. As a matter of fact, in the Fe–Rh [37], Gd–Si–Ge [38], and La–Fe–Si [39] materials with large unit cell volume change (0.9%, 0.4%, 1.3%, respectively) during phase transformation, large magnetic entropy change was also observed. Most remarkably, in the B-doped Mn–Co–Ge alloy with the large unit cell volume change of 4.0% [40], giant magnetic entropy change of about 47.3 J kg^{-1} K^{-1} (under 5 T) was recently reported by Trung et al. [40]. The correlation between the unit cell volume change and magnetic entropy change is helpful for predicting high-performance magnetocaloric materials from the crystallographic data.

Giant Magnetic Refrigeration Capacity Near Room Temperature in $Ni_{40}Co_{10}Mn_{40}Sn_{10}$ Magnetic Shape Memory Alloy

Although the magnitude of ΔS_m under 5 T is very large for the $Ni_{41}Co_9Mn_{40}Sn_{10}$ alloy, its operating temperature window with large ΔS_m is very narrow. For practical applications of the Ni–Mn–*X*-based (*X* = In, Sn, Sb, Ga) magnetocaloric materials, it is urgent to surmount the obstacle of limited operating temperature window. On the other hand, it is of great significance to enhance the refrigeration capacity of these materials to facilitate their more efficient use for magnetic refrigeration. Furthermore, the magnetocaloric effect should occur near room temperature. Thus, in order to meet the above-mentioned requirements, the $\Delta T/\mu_0\Delta H$ should be further enhanced. Therefore, we further tuned the magnetostructural transformation parameters via Co addition. We found that the Curie temperature of austenite (about 446 K, determined from the DSC curve in Fig. 1) of the $Ni_{40}Co_{10}Mn_{40}Sn_{10}$ alloy is increased to a higher temperature and martensitic transformation temperatures are brought down to lower temperatures (near room temperature) (Fig. 1). Therefore, the difference between the Curie temperature of austenite and martensitic transformation temperature is notably enhanced and a larger $\Delta T/\mu_0\Delta H$ can be expected in the $Ni_{40}Co_{10}Mn_{40}Sn_{10}$ alloy according to Ref. [35]. Additionally, this alloy still has a large ΔS_{tr} of 14.1 J kg^{-1} K^{-1} determined from the DSC data as shown in Fig. 1. It should be noted that the thermal hysteresis and phase transformation interval of the $Ni_{40}Co_{10}Mn_{40}Sn_{10}$ alloy are larger than that of the $Ni_{41}Co_9Mn_{40}Sn_{10}$ alloy, as shown in Fig. 1. Similar results were observed in our previous work [35].

In order to determine the value of $\Delta T/\mu_0\Delta H$ and examine the magnetic field-induced phase transformation, we carried out isofield magnetization measurements. The $M(T)$ curves under 0.01 T and 4 T magnetic fields are shown in Fig. 6a and the $M(H)$ curves measured at different temperatures are illustrated in Fig. 6b. It is evident that the high-temperature austenite shows ferromagnetic feature [see the $M(H)$ curve at 350 K in Fig. 6b], while the low-temperature martensite is in a weak magnetic state. Hence, a large magnetization difference between the two phases across martensitic transformation is observed (Fig. 6a). It can be seen from Fig. 6a that application of magnetic fields notably decreases the phase transformation temperatures of the studied alloy. The A_s temperature is decreased by 33 K under a magnetic field of 4 T, with the rate of 8.3 K/T. This is much larger than the values reported in other Ni–(Co)–Mn–Sn alloys [13, 23, 35]. We

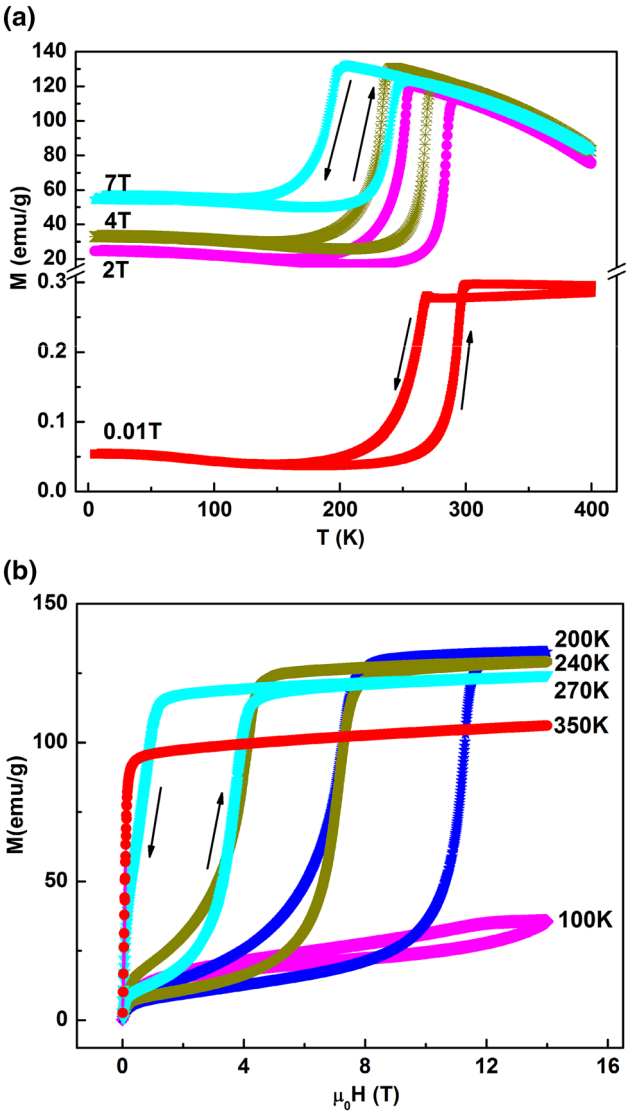

Fig. 6 **a** $M(T)$ curves measured under magnetic fields of 0.01, 2, 4, and 7 T, respectively, for the $Ni_{40}Co_{10}Mn_{40}Sn_{10}$ alloy. **b** $M(H)$ curves measured at 100, 200, 240, 270, and 350 K, respectively, for the $Ni_{40}Co_{10}Mn_{40}Sn_{10}$ alloy. The *arrows* indicate increasing and decreasing magnetic fields during a cycle. Adapted from [24]

also found that the thermal hysteresis in $Ni_{40}Co_{10}Mn_{40}Sn_{10}$ increases with the increase of magnetic field. It is generally acknowledged that the hysteresis behavior is related to the nucleation of new phase and the interfacial interaction at the phase boundary during first-order phase transformation. According to previous work [41], the hysteresis is linked to the friction strength of phase boundary motion during the magnetostructural transformation in Ni–Mn–*X*-based (X = In, Sn, Sb, Ga) Heusler alloys. The increase of hysteresis may suggest that the friction resistance increases with the increase of magnetic field. The value of $\Delta(\mu_0 H)_{com}$ for this alloy is determined to be about 2.2 T according to $\Delta(\mu_0 H)_{com} = (A_f - A_s)/(\Delta T/\mu_0 \Delta H)$ and this value of 2.2 T is far smaller than 4 T obtained in the $Ni_{41}Co_9Mn_{30}Sn_{10}$ alloy. This indicates that the transformation in the $Ni_{40}Co_{10}Mn_{40}Sn_{10}$ alloy can be more easily driven by the magnetic field compared with that in the $Ni_{41}Co_9Mn_{40}Sn_{10}$ alloy. Considering the above-mentioned information, we believe that our $Ni_{40}Co_{10}Mn_{40}Sn_{10}$ alloy shows large ΔS_m with a very broad operating temperature window.

To evaluate the MCE of the studied $Ni_{40}Co_{10}Mn_{40}Sn_{10}$ alloy, we performed isothermal magnetization measurements. The $M(H)$ curves at different temperatures close to the austenitic transformation temperature were recorded and the resultant $M(H)$ curves are shown in Fig. 7a. Correspondingly, ΔS_m was estimated numerically from the isothermal $M(H)$ curves according to the Maxwell relation [Eq. (1)]. The temperature dependence of ΔS_m at different

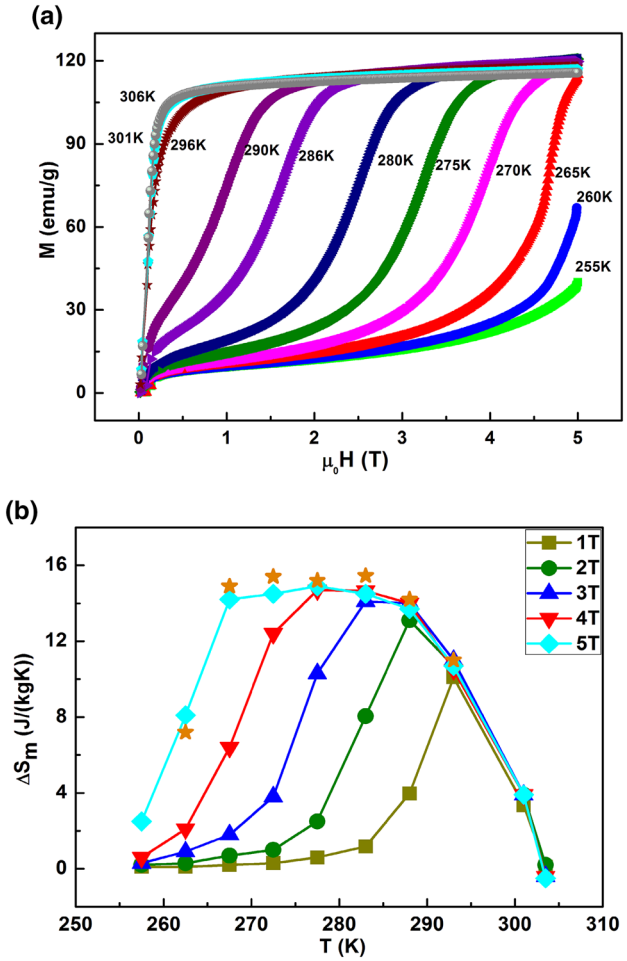

Fig. 7 **a** $M(H)$ curves measured at different temperatures close to the austenitic transformation temperature, for the $Ni_{40}Co_{10}Mn_{40}Sn_{10}$ alloy. For clarity, only the curves during increasing magnetic fields are displayed. **b** The magnetic entropy change (ΔS_m) as a function of temperature at different magnetic fields, for the $Ni_{40}Co_{10}Mn_{40}Sn_{10}$ alloy. The *solid stars* denote the data estimated from the Clausius–Clapeyron relation for a magnetic field of 5 T, while the other solid symbols denote the data calculated using the Maxwell relation for different magnetic fields. Adapted from [24]

magnetic fields is demonstrated in Fig. 7b. It is apparent that the curves show a broad plateau with the maximum value of $\Delta S_m \approx 14.9$ J kg^{-1} K^{-1} under a magnetic field of 5 T, since this magnetic field is large enough to induce complete phase transformation over a wide temperature range. Notably, the plateau covers a broad temperature interval from 267 to 287 K (under 5 T), resulting in an effective operating temperature window of 33 K (determined from the full width half maximum of the ΔS_m peak). The maximum value of ΔS_m (14.9 J kg^{-1} K^{-1}) is in good agreement with the ΔS_{tr} (14.1 J kg^{-1} K^{-1}) determined from DSC. To further validate the ΔS_m we achieved, we also carried out estimation with the Clausius–Clapeyron relation [Eq. (2)], and the obtained results for a field of 5 T are shown as solid stars in Fig. 6b. Clearly, the ΔS_m values estimated with the Maxwell relation and the Clausius–Clapeyron relation are in good agreement, confirming the reliability of our results.

With Eq. (3), the RC value for our $Ni_{40}Co_{10}Mn_{40}Sn_{10}$ alloy was estimated and it is compared with the values for the most studied magnetocaloric materials [26, 28, 32, 42–62], as shown in Fig. 8a. It can be seen that the RC value for the present $Ni_{40}Co_{10}Mn_{40}Sn_{10}$ alloy is significantly larger than that of other Heusler-type Ni–Mn-based magnetocaloric materials. With Eq. (4), RC_{eff} for the studied alloy was calculated to be 251 J kg^{-1} for a magnetic field of 5 T. For comparison, the RC_{eff} values under a field of 5 T for the most studied magnetocaloric materials [26, 28, 32, 42–51, 63] are schematically illustrated in Fig. 8b. It is clear that our $Ni_{40}Co_{10}Mn_{40}Sn_{10}$ alloy shows the largest RC_{eff} among the Ni–Mn-based magnetocaloric materials, and its RC_{eff} value is comparable to that of the most promising Gd–Si–Ge and La–Fe–Si magnetocaloric materials. The large RC_{eff} is beneficial for the magnetic refrigeration applications.

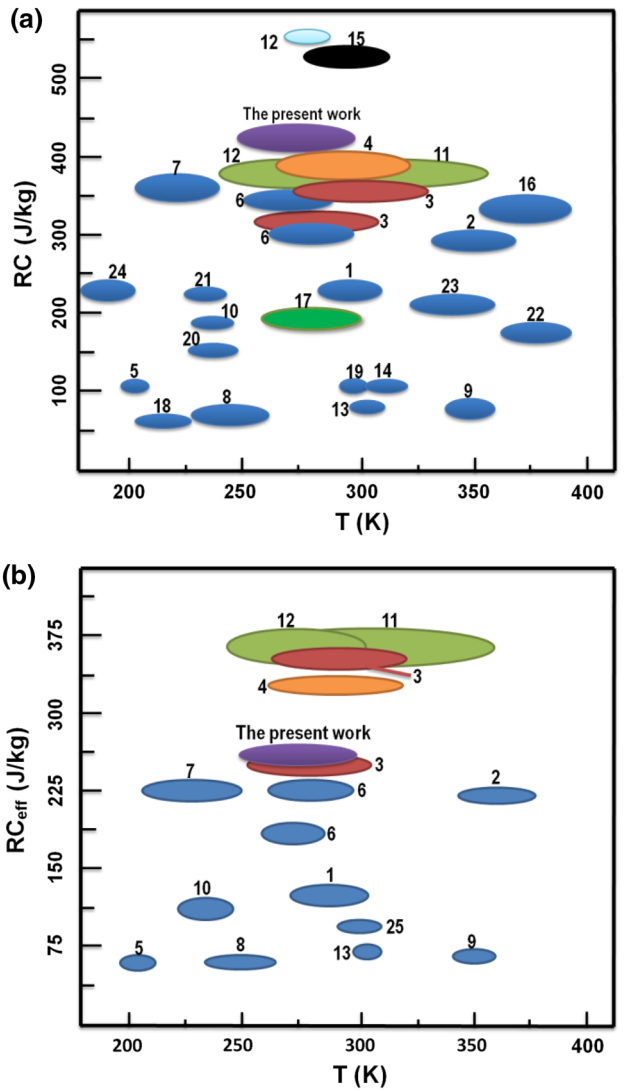

Fig. 8 Schematic illustration of the magnetic refrigeration capacity (RC) (**a**) and the effective magnetic refrigeration capacity (RC_{eff}) (**b**) as a function of temperature under a magnetic field of 5 T for the most studied magnetocaloric materials. Except for the data obtained from the present work (for the $Ni_{40}Co_{10}Mn_{40}Sn_{10}$ alloy), the other data are taken or deduced from the references, with the numbers denoting: 1-$Ni_{45}Co_5Mn_{37}In_{13}$ [43], 2-$Ni_{45}Co_5Mn_{37.5}In_{12.5}$ [26], 3-$Gd_5Si_2Ge_2$/$Gd_5Si_2Ge_{1.9}Fe_{0.1}$ [28], 4-$Fe_{48}Rh_{52}$ [42], 5-$Ni_{42}Co_8Mn_{30}Fe_2Ga_{18}$ [32], 6-$Ni_{45}Co_5Mn_{36.6}In_{13.4}$/$Ni_{45}Co_{4.75}Fe_{0.25}Mn_{36.6}In_{13.4}$ [44], 7-$Ni_{50}Mn_{34}In_{16}$ [45], 8-$Ni_{50}Mn_{37}Sn_{13}$ [46], 9-$Ni_{52}Mn_{26}Ga_{22}$ [47], 10-$Ni_{50}Mn_{34}In_{16}$ [48], 11-$La_{0.7}Pr_{0.3}Fe_{11.5}Si_{1.5}C_{0.2}H_x$ ($x = 0.6$, 1.2) [49], 12-Gd/$La_{1-x}Pr_xFe_{10.7}Co_{0.8}Si_{1.5}$ ($x = 0$, 0.2, 0.4, 0.5) [50], 13-$Ni_2Mn_{0.75}Cu_{0.25}Ga$ [51], 14-$Ni_{50}Mn_{35.3}In_{14.7}$ [52], 15-MnAs [53], 16-$Ni_{45}Co_5Mn_{37.5}In_{12.5}$ [54], 17-$Mn_{0.89}Fe_{0.11}CoGe$ [55], 18-$Ni_2Mn_{1.36}Sn_{0.4}Ga_{0.24}$ [56], 19-$Ni_{50}Mn_{35}In_{15}$ [57], 20-$Ni_{49}Fe_1Mn_{37}Sn_{13}$ [58], 21-$Ni_{44}Fe_2Mn_{43}Sn_{11}$ [59], 22-$Ni_{43}Co_7Mn_{31}Ga_{19}$ [60], 23-$Ni_{41}Co_9Mn_{32}Ga_{16}In_2$ [61], 24-$Ni_{43}Mn_{46}Sn_{11}C_2$ [62], 25-$Ni_{50}Mn_{33}Cr_1In_{16}$ [63]. Adapted from [24]

Large Reversible Magnetocaloric Effect in a Ni–Co–Mn–In Magnetic Shape Memory Alloy with Small Magnetic Hysteresis

For Ni–Mn–*X*-based (X = In, Sn, Sb, Ga) magnetocaloric materials, as mentioned before, their disadvantage is the presence of thermal and magnetic hysteresis which will make them exhibit small or no magnetocaloric effect during the second and subsequent field cycles [11]. To achieve a reversible magnetocaloric effect, the Ni–Mn–*X*-based (X = In, Sn, Sb, Ga) magnetocaloric materials should have small ΔT_{hys}, narrow ΔT_{int}, and large $\Delta T/\mu_0\Delta H$. Among the Ni–Mn–*X*-based (X = In, Sn, Sb, Ga) alloys, Ni–Mn–In-based alloys are easier to meet these demands due to their very small hysteresis, according to the information in literature [21, 64]. Therefore, we select $Ni_{51}Mn_{33.5}In_{15.5}$ as an initial alloy and add Co at the expense of Ni in this Ni–Mn–In alloy.

Figure 9a shows the DSC curve of the $Ni_{49.8}Co_{1.2}Mn_{33.5}In_{15.5}$ alloy. It can be seen that the Curie temperature

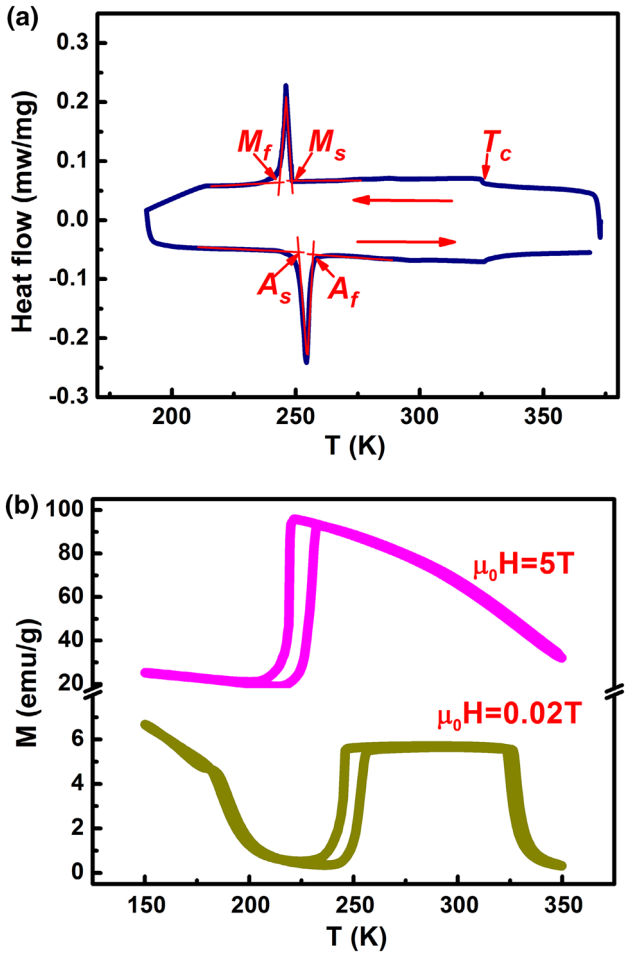

Fig. 9 **a** DSC curves with cooling and heating rates of 10 K/min, for the $Ni_{49.8}Co_{1.2}Mn_{33.5}In_{15.5}$ alloy. The *horizontal arrows* indicate the cooling and heating processes. The determination of the transformation temperatures, M_s, M_f, A_s, A_f, and T_c, is illustrated on the curves. **b** $M(T)$ curves measured under magnetic fields of 0.02 and 5 T, respectively, for the $Ni_{49.8}Co_{1.2}Mn_{33.5}In_{15.5}$ alloy. Adapted from [25]

is 325.7 K, while the martensitic and austenitic transformation start and finish temperatures, M_s, M_f, A_s, and A_f, are 248.7, 243.4, 251.1, and 256.8 K, respectively. Correspondingly, the thermal hysteresis is $A_f - M_s = 8.1$ K (or $A_s - M_f = 7.7$ K) and transformation interval is $M_s - M_f = 5.3$ K(or $A_f - A_s = 5.7$ K). Additionally, the ΔS_{tr} is determined to be 14.4 J kg^{-1} K^{-1} from the DSC data. Figure 9b shows the $M(T)$ curves measured under 0.02 T and 5 T, respectively. From the $M(T)$ curve under 5 T, a large magnetization difference ($\Delta M \approx 75.4$ emu/g) between the two phases across martensitic transformation can be determined. It can be seen that A_s is decreased by 24.5 K by a field of 5 T, with the rate of $\Delta A_s/\mu_0\Delta H \approx 4.9$ K/T. It is reported that a reversible MCE can be obtained in a certain temperature interval when the magnitude of the shift in martensitic transformation temperatures induced by the magnetic field is larger than the sum of the thermal hysteresis and transformation interval [21]. That is to say, a reversible MCE occurs in a certain temperature interval when there is a gap between the $M(T)$ hysteresis loop under magnetic field and that under zero field. We indeed found a gap between the hysteresis loop under 5 T and that under 0.02 T (Fig. 9b), which corresponds to the temperature interval between 225.7 K (the A_s under 5 T) and 242.1 K (the M_f under 0.02 T). Thus, a reversible MCE could be achieved within this temperature interval in our $Ni_{49.8}Co_{1.2}Mn_{33.5}In_{15.5}$ alloy.

To evaluate the reversibility of the magnetic field-induced transformation, we carried out $M(H)$ measurements in the temperature range of 222–240 K at an interval of 3 K during the cyclic increasing and decreasing magnetic field, as shown in Fig. 10a. It can be found that at each temperature, the $M(H)$ curves recorded during the first and second cycles of increasing and decreasing magnetic field almost coincide with each other (Fig. 10a). This suggests that there is no residual field-induced austenite after each cycle and the transformation induced by magnetic field at these temperatures is almost fully reversible, which could lead to a reversible MCE. It can also be found that the magnetic hysteresis (ΔH_{hy}) is very small ($\approx$1.1 T) in our $Ni_{49.8}Co_{1.2}Mn_{33.5}In_{15.5}$ alloy, which is marked by the horizontal arrow in Fig. 10a. In order to compare the magnetic hysteresis in the present $Ni_{49.8}Co_{1.2}Mn_{33.5}In_{15.5}$ alloy with that in other magnetocaloric materials in literature [14, 19, 24, 26, 43, 64–73], the magnetic hysteresis of Ni–(Co)–Mn–X (X = In, Sn, Sb) Heusler alloys is shown in Fig. 10b. Obviously, our $Ni_{49.8}Co_{1.2}Mn_{33.5}In_{15.5}$ alloy shows the minimum magnetic hysteresis ($\approx$1.1 T) among the Ni–Mn–X-based (X = In, Sn, Sb, Ga) magnetocaloric materials. The small magnetic hysteresis is important for reducing the energy loss during magnetic field cycling and attaining a large reversible MCE.

The temperature dependence of the reversible magnetic entropy change (ΔS_m) under 5 T, estimated with the Maxwell relation [see Eq. (1)] based on the $M(H)$ data shown in Fig. 11a, is depicted in Fig. 11b. It can be seen that the maximum value of ΔS_m under 5 T is about 14.6 J kg^{-1} K^{-1}. To further verify the validity of our data, we also estimated the ΔS_m values with the Clausius–Clapeyron relation which applies to the first-order phase transformation [see Eq. (2)], and such values are shown in Fig. 11b as solid stars. A good agreement between the values estimated with the Clausius–Clapeyron relation and the Maxwell relation is observed, confirming the reliability of the data. The reversible magnetic refrigeration capacity (RC) is estimated with Eq. (3) to be 125.0 J kg^{-1}. Thanks to the small magnetic hysteresis, the present $Ni_{49.8}Co_{1.2}Mn_{33.5}In_{15.5}$ alloy only exhibits a low average magnetic hysteresis ($\overline{HL}$) of 48.4 J kg^{-1}. Therefore, according to

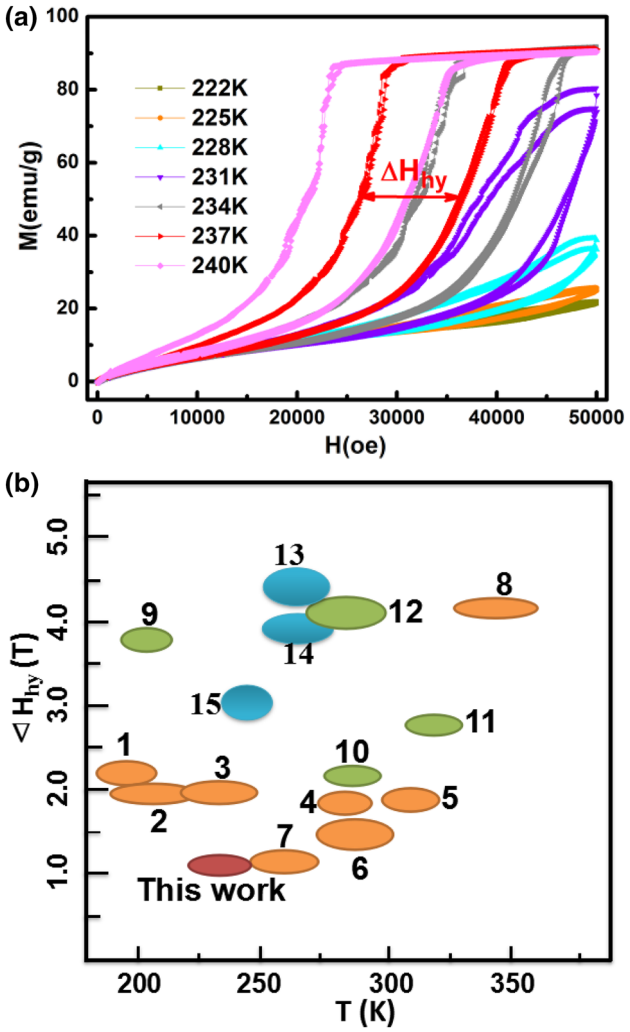

Fig. 10 **a** Two cycles of isothermal $M(H)$ curves with minor difference between the first and second cycles at constant temperatures from 222 to 240 K with an interval of 3 K, for the $Ni_{49.8}Co_{1.2}Mn_{33.5}In_{15.5}$ alloy. **b** Schematic illustration of the magnetic hysteresis as a function of temperature for Ni–(Co)–Mn–X (X = In, Sn, Sb) Heusler alloys. Except for the data obtained from the present work (for the $Ni_{49.8}Co_{1.2}Mn_{33.5}In_{15.5}$ alloy), the other data are taken or deduced from the references, with the numbers denoting: 1-$Ni_{50.3}Mn_{33.8}In_{15.9}$ [71], 2-$Ni_{50}Mn_{35}In_{15}$ [66], 3-$Ni_{50}Mn_{34}In_{16}$ [72], 4-$Ni_{45}Co_5Mn_{36.7}In_{13.3}$ [14], 5-$Ni_{45}Co_5Mn_{37}In_{13}$ [43], 6-$Ni_{50}Mn_{35}In_{15}$ [73], 7-$Ni_{51}Mn_{33}In_{16}$ [64], 8-$Ni_{45}Co_5Mn_{37.5}In_{12.5}$ [26], 9-$Ni_{43}Co_4Mn_{42}Sn_{11}$ [19], 10-$Ni_{43}Co_7Mn_{39}Sn_{11}$ [70], 11-$Ni_{43.5}Co_{6.5}Mn_{39}Sn_{11}$ [69], 12-$Ni_{40}Co_{10}Mn_{40}Sn_{10}$ [24], 13-$Ni_{45}Co_5Mn_{38}Sb_{12}$ [68], 14-$Ni_{45}Co_5Mn_{38}Sb_{12}$ [67], 15-$Ni_{50}Co_5Mn_{39}Sb_{11}$ [65]. Adapted from [25]

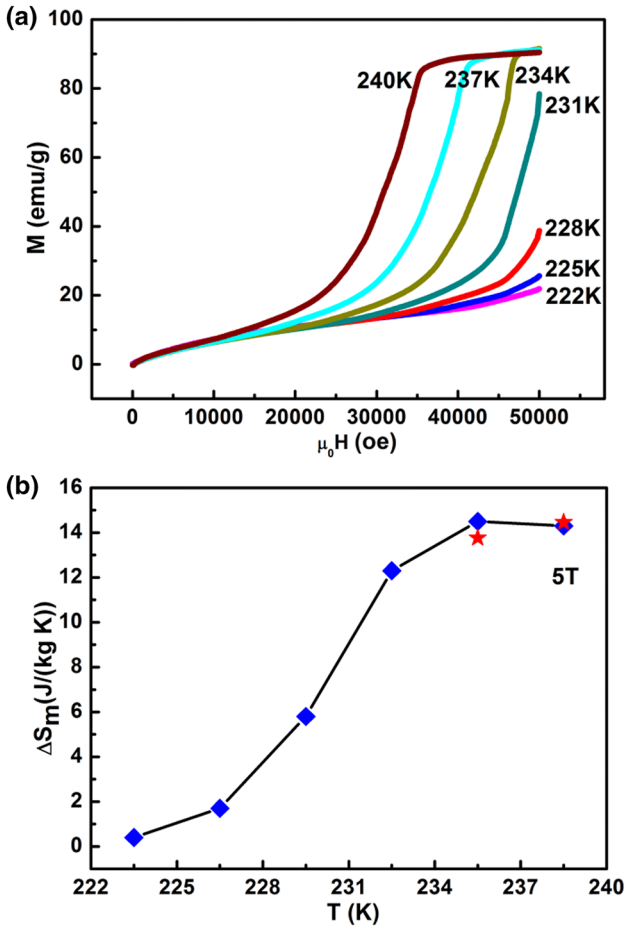

Fig. 11 **a** $M(H)$ curves measured at different temperatures from 222 to 240 K with an interval of 3 K, for the $Ni_{49.8}Co_{1.2}Mn_{33.5}In_{15.5}$ alloy. For clarity, only the curves recorded during increasing magnetic fields are shown. **b** The reversible magnetic entropy change (ΔS_m) under a magnetic field of 5 T shown as a function of temperature, for the $Ni_{49.8}Co_{1.2}Mn_{33.5}In_{15.5}$ alloy. The *solid stars* denote the data estimated from the Clausius–Clapeyron relation. Adapted from [25]

Eq. (4), the reversible magnetic refrigeration capacity RC_{eff} is determined to be 76.6 J kg^{-1}. Actually, this is a large reversible RC_{eff}, beneficial for practical magnetic refrigeration applications.

The reversibility of phase transformation is especially crucial for a magnetic refrigerant like Ni–Mn–X-based (X = In, Sn, Sb, Ga) Heusler alloys which undergo first-order magnetostructural transformation. Because of the large hysteresis or the very small sensitivity of transition temperature to the applied magnetic field in many of the Ni–Mn-based Heusler alloys reported in literature, the austenite induced by the magnetic field cannot transform back to the initial martensite when the magnetic field is removed. Fortunately, we achieved a large reversible MCE in our $Ni_{49.8}Co_{1.2}Mn_{33.5}In_{15.5}$ alloy by tuning its magnetostructural transformation parameters. Nevertheless, it should be noted that this large reversible MCE was achieved under a magnetic field of 5 T. From the practical application point of view, large reversible MCE should be achieved at relatively low fields that could be provided by permanent magnets. In order to achieve this goal, it is essential to further reduce the thermal hysteresis and phase transformation interval and enhance the sensitivity of phase transformation temperature to applied magnetic field. Recently, barocaloric effect and elastocaloric effect have also been reported in Ni–Mn-based magnetic shape

memory alloys [74]. The multicaloric effects observed in these alloys may imply that the MCE can be tailored by uniaxial stress or hydrostatic pressure. We expect that large reversible MCE could be obtained under low magnetic fields via a dual-stimulus multicaloric cycle.

Conclusions and Extension Remarks

Investigation on MCE is of great significance for not only fundamental interests but also technological applications. Recently, we have investigated the MCE in Ni–Mn–Sn-based and Ni–Mn–In-based magnetic shape memory alloys. In these alloys, thermal hysteresis, phase transformation interval, and the sensitivity of phase transformation temperature to applied magnetic field are not only interdependent but also increase simultaneously with the decrease of phase transformation temperature caused either by magnetic field or by composition variation. It is difficult to optimize the magnetocaloric properties due to the interdependence of these magnetostructural transformation parameters. In this paper, we demonstrated our recent work on developing high-performance magnetocaloric materials in Ni–Co–Mn–Sn and Ni–Co–Mn–In magnetic shape memory alloy systems. By systematically tuning the magnetostructural transformation parameters via Co substitution in Ni–Mn–Sn-based and Ni–Mn–In-based alloys, a variety of novel magnetocaloric properties have been developed. A large magnetic entropy change of 31.9 J kg^{-1} K^{-1} under 5 T was obtained in the $Ni_{41}Co_9Mn_{40}Sn_{10}$ alloy. A giant effective magnetic refrigeration capacity of 251 J kg^{-1} under 5 T and a broad operating temperature window of 33 K near room temperature were achieved in the $Ni_{40}Co_{10}Mn_{40}Sn_{10}$ alloy. A large reversible magnetic entropy change of 14.6 J kg^{-1} K^{-1} and a broad operating temperature window of 18 K were achieved under 5 T in the $Ni_{49.8}Co_{1.2}Mn_{33.5}In_{15.5}$ magnetic shape memory alloy. Furthermore, a large reversible effective refrigeration capacity of 76.6 J kg^{-1} was obtained under 5 T in this alloy. Additionally, these alloys only consist of inexpensive and non-toxic elements. All these merits make the above-mentioned magnetic shape memory alloys attractive candidates for magnetic refrigeration. In the future, further reducing the critical field required for complete and reversible field-induced transformation to the field range that can be generated by permanent magnets would greatly benefit the practical magnetocaloric refrigeration applications of these materials. To achieve this goal, further increasing the magnetization difference between the two phases (ΔM) and decreasing the thermal hysteresis and phase transformation interval would be required. ΔM may be increased by enhancing the ferromagnetic exchange interaction to increase the Curie temperature and thus enlarge the difference between Curie temperature and phase transformation temperature. The thermal hysteresis and phase transformation interval may be reduced by improving the geometric compatibility between the two phases [75] and/or employing the minor hysteresis loops [17]. THERMAG VI held in 2014 at the Victoria Conference Centre, Canada announced an enhanced scope that includes all magnetocaloric materials and applications, regardless of temperature range [76]. This allows for coverage of new applications such as gas liquefaction systems as well as thermally driven magnetic heat engines. From this point of view, magnetic cooling techniques will be advanced in much wider application fields [76]. Thus, we expect that the balanced tuning of magnetostructural transformation parameters of magnetocaloric alloys provides an instructive reference to the magnetic refrigeration community. The exploration of the multicaloric effect in magnetic shape memory alloys will be a future research trend for solid-state refrigeration.

Acknowledgments This work is supported by the National Natural Science Foundation of China (Nos. 51471030, 11305008, and 51527801), the National High Technology Research and Development Program of China (863 Program) (No. 2015AA034101), the Fundamental Research Funds for the Central Universities (Nos. 06111023 and 06111020), and also supported by State Key Laboratory for Advanced Metals and Materials (Grant Nos. 2016-T01 and 2015-ZD01).

References

1. Pecharsky VK, Gschneidner KA Jr (1999) Magnetocaloric effect and magnetic refrigeration. J Magn Magn Mater 200:44–56
2. Gutfleisch O, Willard MA, Brück E, Chen CH, Sankar SG, Liu JP (2011) Magnetic materials and devices for the 21st century: stronger, lighter, and more energy efficient. Adv Mater 23:821–842
3. Chirkova A, Skokov KP, Schultz L, Baranov NV, Gutfleisch O, Woodcock TG (2015) Giant adiabatic temperature change in FeRh alloys evidenced by direct measurements under cyclic conditions. Acta Mater 106:15–21
4. Kitanovski A, Tuek J, Tomc U, Plaznik U, Ozbolt M, Poredo A (2014) Magnetocaloric energy conversion: from theory to applications. Springer International Publishing, Cham
5. Pecharsky VK, Gschneidner KA Jr (1997) Giant magnetocaloric effect in $Gd_5(Si_2Ge_2)$. Phys Rev Lett 78:4494–4497
6. Liu J, Krautz M, Skokov K, Woodcock TG, Gutfleisch O (2011) Systematic study of the microstructure, entropy change and adiabatic temperature change in optimized La-Fe-Si alloys. Acta Mater 59:3602–3611
7. Stern-Taulats E, Gracià-Condal A, Planes A, Lloveras P, Barrio M, Tamarit J-L, Pramanick S, Majumdar S, Mañosa L (2015) Reversible adiabatic temperature changes at the magnetocaloric and barocaloric effects in $Fe_{49}Rh_{51}$. Appl Phys Lett 107:152409
8. Tegus O, Brück E, Buschow KHJ, de Boer FR (2002) Transition-metal-based magnetic refrigerants for room-temperature applications. Nature 415:150–152
9. Liu J, Skokov K, Gutfleisch O (2012) Magnetostructural transition and adiabatic temperature change in Mn-Co-Ge magnetic refrigerants. Scr Mater 66:642

10. Li ZB, Zou NF, Sánchez-Valdés CF, Sánchez Llamazares JL, Yang B, Hu Y, Zhang YD, Esling C, Zhao X, Zuo L (2016) Thermal and magnetic field-induced martensitic transformation in $Ni_{50}Mn_{25-x}Ga_{25}Cu_x$ ($0 \leq x \leq 7$) melt-spun ribbons. J Phys D Appl Phys 49:025002
11. Liu J, Gottschall T, Skokov KP, Moore JD, Gutfleisch O (2012) Giant magnetocaloric effect driven by structural transitions. Nat Mater 11:620–626
12. Nayak AK, Suresh KG, Nigam AK (2009) Giant inverse magnetocaloric effect near room temperature in Co substituted NiMnSb Heusler alloys. J Phys D Appl Phys 42:035009
13. Krenke T, Duman E, Acet M, Wassermann EF, Moya X, Manosa L, Planes A (2005) Inverse magnetocaloric effect in ferromagnetic Ni-Mn-Sn alloys. Nat Mater 4(6):450
14. Kainuma R, Imano Y, Ito W, Sutou Y, Morito H, Okamoto S, Kitakami O, Oikawa K, Fujita A, Kanomata T, Ishida K (2006) Magnetic-field-induced phase recovery by reverse phase transformation. Nature 439:957–960
15. Yu SY, Liu ZH, Liu GD, Chen JL, Cao ZX, Wu GH, Zhang B, Zhang XX (2006) Large magnetoresistance in single-crystalline $Ni_{50}Mn_{50-x}In_x$ alloys ($x = 14$–16) upon martensitic transformation. Appl Phys Lett 89:162503
16. Zhao DW, Liu J, Feng Y, Sun W, Yan AR (2017) Giant elastocaloric effect and its irreversibility in [001]-oriented $Ni_{45}Mn_{36.5}In_{13.5}Co_5$ meta-magnetic shape memory alloys. Appl Phys Lett 110:021906
17. Gottschall T, Skokov KP, Burriel R, Gutfleisch O (2016) On the S(T) diagram of magnetocaloric materials with first-order transition: Kinetic and cyclic effects of Heusler alloys. Acta Mater 107:1–8
18. Mcleod MV, Giri AK, Paterson BA, Dennis CL, Zhou L, Vogel SC, Gourdon O, Reiche HM, Cho KC, Sohn YH, Shull RD, Majumdar BS (2015) Magnetocaloric response of non-stoichiometric Ni_2MnGa alloys and the influence of crystallographic texture. Acta Mater 97:245–256
19. Bruno NM, Yegin C, Karaman I, Chen JH, Ross JH Jr, Liu J, Li JG (2014) The effect of heat treatments on $Ni_{43}Mn_{42}Co_4Sn_{11}$ metamagnetic shape memory alloys for magnetic refrigeration. Acta Mater 74:66–84
20. Tian FH, Zeng YY, Xu MW, Yang S, Lu T, Wang JQ, Chang TY, Adil M, Zhang Y, Zhou C, Song XP (2015) A magnetocaloric effect arising from a ferromagnetic transition in the martensitic state in Heusler alloy of $Ni_{50}Mn_{36}Sb_8Ga_6$. Appl Phys Lett 107:012406
21. Stern-Taulats E, Castillo-Villa PO, Mañosa L, Frontera C, Pramanick S, Majumdar S, Planes A (2014) Magnetocaloric effect in the low hysteresis Ni-Mn-In metamagnetic shape memory Heusler alloy. J Appl Phys 115:173907
22. Gottschall T, Skokov KP, Benke D, Gruner ME, Gutfleisch O (2016) Contradictory role of the magnetic contribution in inverse magnetocaloric Heusler materials. Phys Rev B 93:184431
23. Huang L, Cong DY, Ma L, Nie ZH, Wang MG, Wang ZL, Suo HL, Ren Y, Wang YD (2015) Large magnetic entropy change and magnetoresistance in a $Ni_{41}Co_9Mn_{40}Sn_{10}$ magnetic shape memory alloy. J Alloys Compd 647:1081–1085
24. Huang L, Cong DY, Suo HL, Wang YD (2014) Giant magnetic refrigeration capacity near room temperature in $Ni_{40}Co_{10}Mn_{40}Sn_{10}$ multifunctional alloy. Appl Phys Lett 104:132407
25. Huang L, Cong DY, Ma L, Nie ZH, Wang ZL, Suo HL, Ren Y, Wang YD (2016) Large reversible magnetocaloric effect in a Ni-Co-Mn-In magnetic shape memory alloy. Appl Phys Lett 108:032405
26. Bourgault D, Tillier J, Courtois P, Maillard D, Chaud X (2010) Large inverse magnetocaloric effect in $Ni_{45}Co_5Mn_{37.5}In_{12.5}$ single crystal above 300 K. Appl Phys Lett 96:132501
27. Balli M, Fruchart D, Gignoux D, Zach R (2009) The "colosssal" magnetocaloric effect in $Mn_{1-x}Fe_xAs$: What are we really measuring? Appl Phys Lett 95:072509
28. Provenzano V, Shapiro AJ, Shull RD (2004) Reduction of hysteresis losses in the magnetic refrigerant $Gd_5Ge_2Si_2$ by the addition of iron. Nature 429:853
29. Yang LH, Zhang H, Hu FX, Sun JR, Pan LQ, Shen BG (2014) Magnetocaloric effect and martensitic transition in $Ni_{50}Mn_{36-x}Co_xSn_{14}$. J Alloys Compd 588:46–48
30. Pathak AK, Khan M, Dubenko I, Stadler S, Ali N (2007) Large magnetic entropy change in $Ni_{50}Mn_{50-x}In_x$ Heusler alloys. Appl Phys Lett 90:262504
31. Han ZD, Wang DH, Zhang CL, Tang SL, Gu BX, Du YW (2006) Large magnetic entropy changes in $Ni_{45.4}Mn_{41.5}In_{13.1}$ ferromagnetic shape memory alloy. Appl Phys Lett 89:182507
32. Pathak AK, Dubenko I, Karaca HE, Stadler S, Ali N (2010) Large inverse magnetic entropy changes and magnetoresistance in the vicinity of a field-induced martensitic transformation in $Ni_{50-x}Co_xMn_{32-y}Fe_yGa_{18}$. Appl Phys Lett 97:062505
33. Xuan HC, Wang DH, Zhang CL, Han ZD, Gu BX, Du YW (2008) Boron's effect on martensitic transformation and magnetocaloric effect in $Ni_{43}Mn_{46}Sn_{11}B_x$ alloys. Appl Phys Lett 92:102503
34. Emre NM, Bruno SY, Emre I (2014) Karaman, Effect of niobium addition on the martensitic transformation and magnetocaloric effect in low hysteresis NiCoMnSn magnetic shape memory alloys. Appl Phys Lett 105:231910
35. Cong DY, Roth S, Schultz L (2012) Magnetic properties and structural transformations in Ni–Co–Mn–Sn multifunctional alloys. Acta Mater 60:5335–5351
36. Karaca HE, Karaman I, Basaran B, Ren Y, Chumlyakov YI, Maier HJ (2009) Magnetic field-induced phase transformation in NiMnCoIn magnetic shape memory alloys—a new actuation mechanism with large work output. Adv Funct Mater 19:983–998
37. Algarabel PA, Ibarra MR, Marquina C, Del Moral A, Galibert J, Iqbal M, Askenazy S (1995) Giant room-temperature magnetoresistance in the FeRh alloy. Appl Phys Lett 66:3062–3064
38. Morellon L, Algarabel PA, Lbarra MR, Blasco J, Garcia-Landa B, Arnold Z, Albertini F (1998) Magnetic-field-induced structural phase transition in $Gd_5(Si_{1.8}Ge_{2.2})$. Phys Rev B 58:R14721
39. Hu FX, Shen BG, Sun JR, Wang GJ, Cheng ZH (2002) Very large magnetic entropy change near room temperature in $LaFe_{11.2}Co_{0.7}Si_{1.1}$. Appl Phys Lett 80:826
40. Trung NT, Zhang L, Caron L, Buschow KHJ, Brück E (2010) Giant magnetocaloric effects by tailoring the phase transitions. Appl Phys Lett 96:172504
41. Wang WH, Chen JL, Liu ZH, Wu GH, Zhan WS (2002) Thermal hysteresis and friction of phase boundary motion in ferromagnetic $Ni_{52}Mn_{23}Ga_{25}$ single crystals. Phys. Rev. B 65:012416
42. Manekar M, Roy SB (2008) Reproducible room temperature giant magnetocaloric effect in Fe-Rh. J Phys D Appl Phys 41:192004
43. Liu J, Scheerbaum N, Lyubina J, Gutfleisch O (2008) Reversibility of magnetostructural transition and associated magnetocaloric effect in Ni-Mn-In-Co. Appl Phys Lett 93:102512
44. Chen L, Hu FX, Wang J, Bao LF, Sun JR, Shen BG, Yin JH, Pan LQ (2012) Magnetoresistance and magnetocaloric properties involving strong metamagnetic behavior in Fe-doped $Ni_{45}(Co_{1-x}Fe_x)_5Mn_{36.6}In_{13.4}$ alloys. Appl Phys Lett 101:012401
45. Chattopadhyay MK, Sharma VK, Roy SB (2008) Thermomagnetic history dependence of magnetocaloric effect in $Ni_{50}Mn_{34}In_{16}$. Appl Phys Lett 92:022503
46. Phan T-L, Zhang P, Dan NH, Yen NH, Thanh PT, Thanh TD, Phan MH, Yu SC (2012) Coexistence of conventional and inverse magnetocaloric effects and critical behaviors in $Ni_{50}Mn_{50-x}Sn_x$ ($x = 13$ and 14) alloy ribbons. Appl Phys Lett 101:212403

47. Li ZB, Zhang YD, Sánchez-Valdés CF, Sánchez Llamazares JL, Esling C, Zhao X, Zuo L (2014) Giant magnetocaloric effect in melt-spun Ni-Mn-Ga ribbons with magneto-multistructural transformation. Appl Phys Lett 104:044101
48. Sharma VK, Chattopadhyay MK, Roy SB (2007) Large inverse magnetocaloric effect in $Ni_{50}Mn_{34}In_{16}$. J Phys D Appl Phys 40:1869–1873
49. Zhao JL, Shen J, Zhang H, Xu ZY, Wu JF, Hu FX, Sun JR, Shen BG (2012) Hydrogenating process and magnetocaloric effect in $La_{0.7}Pr_{0.3}Fe_{11.5}Si_{1.5}C_{0.2}H_x$ hydrides. J. Alloys Compd. 520:277–280
50. Shen J, Gao B, Dong QY, Li YX, Hu FX, Sun JR, Shen BG (2008) $La_{1-x}Pr_xFe_{10.7}Co_{0.8}Si_{1.5}$ compounds near room temperature. J Phys D Appl Phys 41:245005
51. Stadler S, Khan M, Mitchell J, Ali N, Gomes AM, Dubenko I, Takeuchi AY, Guimarães AP (2006) Magnetocaloric properties of $Ni_2Mn_{1-x}Cu_xGa$. Appl Phys Lett 88:192511
52. Zhang XX, Zhang B, Yu SY, Liu ZH, Xu WJ, Liu GD, Chen JL, Cao ZX, Wu GH (2007) Combined giant inverse and normal magnetocaloric effect for room-temperature magnetic cooling. Phys Rev B 76:132403
53. Magnus G, Carvalho AA, Coelho PJ Von, Ranke SC (2011) Alves, The isothermal variation of the entropy change (ΔS_T) may be miscalculated from magnetization isotherms in some cases: MnAs and $Gd_5Ge_2Si_2$ compounds as examples. J Alloys Compd 509:3452–3456
54. Guillou F, Courtois P, Porcar L, Plaindoux P, Bourgault D, Hardy V (2012) Calorimetric investigation of the magnetocaloric effect in $Ni_{45}Co_5Mn_{37.5}In_{12.5}$. J Phys D Appl Phys 40:255001
55. Wang ZL, Nie ZH, Zeng JX, Su R, Zhang YP, Brown DE, Ren Y, Wang YD (2013) First-order magnetostructural transformation in Fe doped Mn-Co-Ge alloys. J Alloys Compd 577:486–490
56. Chatterjee S, Giri S, De SK, Majumdar S (2010) Giant magnetocaloric effect near room temperature in Ni-Mn-Sn-Ga alloys. J Alloys Compd 503:273–276
57. Bhobe PA, Priolkar KR, Nigam AK (2007) Room temperature magnetocaloric effect in Ni-Mn-In. Appl Phys Lett 91:242503
58. Krenke T, Duman E, Acet M, Moya X, Mañosa L, Planes A (2007) Effect of Co and Fe on the inverse magnetocaloric properties of Ni-Mn-Sn. J Appl Phys 102:033903
59. Zhao XG, Tong M, Shih CW, Li B, Chang WC, Liu W, Zhang ZD (2013) Microstructure, martensitic transitions, magnetocaloric, and exchange bias properties in Fe-doped Ni-Mn-Sn melt-spun ribbons. J Appl Phys 113:17A913
60. Fabbrici S, Kamarad J, Arnold Z, Casoli F, Paoluzi A, Bolzoni F, Cabassi R, Solzi M, Porcari G, Pernechele C, Albertini F (2011) From direct to inverse giant magnetocaloric effect in Co-doped NiMnGa multifunctional alloys. Acta Mater 59:412–419
61. Porcari G, Fabbrici S, Pernechele C, Albertini F, Buzzi M, Paoluzi A, Kamarad J, Arnold Z, Solzi M (2012) Reverse magnetostructural transformation and adiabatic temperature change in Co- and In-substituted Ni-Mn-Ga alloys. Phys Rev B 85:024414
62. Zhang Y, Liu J, Zheng Q, Zhang J, Xia WX, Du J, Yan AR (2014) Large magnetic entropy change and enhanced mechanical properties of Ni-Mn-Sn-C alloys. Scr. Mater. 75:26–29
63. Sharma VK, Chattopadhyay MK, Sharath Chandra LS, Roy SB (2011) Elevating the temperature regime of the large magnetocaloric effect in a Ni-Mn-In alloy towards room temperature. J Phys D: Appl Phys 44:145002
64. Hu FX, Wang J, Shen J, Gao B, Sun JR, Shen BG (2009) Large magnetic entropy change with small thermal hysteresis near room temperature in metamagnetic alloys $Ni_{51}Mn_{49-x}In_x$. J Appl Phys 105:07A940
65. Yu SY, Ma L, Liu GD, Liu ZH, Chen JL, Cao ZX, Wu GH, Zhang B, Zhang XX (2007) Magnetic field-induced martensitic transformation and large magnetoresistance in NiCoMnSb alloys. Appl Phys Lett 90:242501
66. Zavareh MG, Mejía CS, Nayak AK, Skourski Y, Wosnitza J, Felser C, Nicklas M (2015) Direct measurements of the magnetocaloric effect in pulsed magnetic fields: The example of the Heusler alloy $Ni_{50}Mn_{35}In_{15}$. Appl Phys Lett 106:071904
67. Nayak AK, Suresh KG, Nigam AK (2011) Anomalous effects of repeated martensitic transition on the transport, magnetic and thermal properties in Ni-Co-Mn-Sb Heusler alloy. Acta Mater 59:3304–3312
68. Nayak AK, Suresh KG, Nigam AK (2010) Irreversibility of field-induced magnetostructural transition in NiCoMnSb shape memory alloy revealed by magnetization, transport and heat capacity studies. Appl Phys Lett 96:112503
69. Cong DY, Roth S, Liu J, Luo Q, Pötschke M, Hürrich C, Schultz L (2010) Superparamagnetic and superspin glass behaviors in the martensitic state of $Ni_{43.5}Co_{6.5}Mn_{39}Sn_{11}$ magnetic shape memory alloy. Appl Phys Lett 96:112504
70. Kainuma R, Imano Y, Ito W, Morito H, Sutou Y, Oikawa K, Fujita A, Ishida K, Okamoto S, Kitakami O, Kanomata T (2006) Metamagnetic shape memory effect in a Heusler-type $Ni_{43}Co_7Mn_{39}Sn_{11}$ polycrystalline alloy. Appl Phys Lett 88:192513
71. Krenke T, Duman E, Acet M, Wassermann EF, Moya X, Mañosa L, Planes A, Suard E, Ouladdiaf B (2007) Magnetic superelasticity and inverse magnetocaloric effect in Ni-Mn-In. Phys Rev B 75:104414
72. Sharma VK, Chattopadhyay MK, Kumar R, Ganguli T, Tiwari P, Roy SB (2007) Magnetocaloric effect in Heusler alloys $Ni_{50}Mn_{34}In_{16}$ and $Ni_{50}Mn_{34}Sn_{16}$. J Phys: Condens Matter 19:496207
73. Li WJ, Ren Q, Zhang XK, Lv XG, Liu H, Meng J, Li D, Li ZD (2009) Zhang, Magnetostructural coupling and magnetocaloric effect in Ni-Mn-In. Appl Phys Lett 95:172506
74. Stern-Taulats E, Planes A, Lloveras P, Barrio M, Tamarit J-L, Pramanick S, Majumdar S, Yüce S, Emre B, Frontera C, Mañosa L (2015) Tailoring barocaloric and magnetocaloric properties in low-hysteresis magnetic shape memory alloys. Acta Mater 96:324–332
75. Song Y, Chen X, Dadabe V, Shield TW, James RD (2013) Enhanced reversibility and unusual microstructure of a phase-transforming material. Nature 502:85–88
76. Liu J (2014) Optimizing and fabricating magnetocaloric materials. Chin Phys B 23:047503